X-Ray Image Detector Based on Light Guides and Scintillators

J. G. Rocha, R. A. Dias, L. Goncalves, G. Minas, *Member, IEEE*, A. Ferreira, C. M. Costa, and S. Lanceros-Mendez

***Abstract*—This paper reports on a study concerning the design of an X-ray detector that is suitable to analyze a small area with high spatial resolution. The indirect method of X-ray detection is used, i.e., the X-rays are first converted into visible light, which is then detected. In this design, an array of CsI:Tl scintillators, encapsulated by aluminum walls, is coupled with an array of CMOS photodetectors. This structure, patented and described theoretically by the authors in previous works, can be obtained using the SU-8 negative photoresist as a sacrificial layer. The experimental work consisted in the deposition of a scintillator layer, and an aluminum layer on the active area of a commercially available digital imaging sensor, thus supporting the developed detector design. X-ray imaging tests were performed using the PHILIPS X'Pert equipment. Promising results were obtained, featuring high resolution and detail.**

***Index Terms*—Photolithography, scintillation detectors, X-ray detectors, X-ray image sensors.**

I. Introduction

DIGITAL radiography is widely replacing traditional radiography. As a major health care area, radiology is also an important research field. The X-ray detectors are currently undergoing fast development toward the attainment of digital radiographies with improved spatial resolution while reducing the radiation dose applied to the patients. There are two main methods to construct X-ray detection systems, known as direct and indirect approaches [1]. The direct method normally uses a photoconductor that is directly exposed to the X-rays. In the indirect method, a scintillator is placed on the top of a photodetector. The scintillator absorbs the X-ray energy and produces visible light, which is detected by the photodetector. This method, being simple, encounters limitations regarding the spatial resolution due to scintillator thickness constraints. Fig. 1 illustrates that as the scintillator thickness increases (which is desirable in order to absorb more X-ray photons to be converted into visible light), the spatial resolution decreases [2].

Manuscript received December 04, 2008; revised March 04, 2009; accepted March 09, 2009. Current version published August 21, 2009. This work was supported in part by the Portuguese Institute of Industrial Property (INPI)—SIUPI program. This is an expanded paper from the Sensors 2008 Conference. The associate editor coordinating the review of this paper and approving it for publication was Prof. Masayoshi Esashi.

J. G. Rocha, R. A. Dias, L. Goncalves, and G. Minas are with the Department of Industrial Electronics, University of Minho, Campus de Azurem, Guimarães 4800, Portugal (e-mail: gerardo@dei.uminho.pt).

A. Ferreira, C. M. Costa, and S. Lanceros-Mendez are with the Department of Physics, University of Minho, Campus de Gualtar, Braga 4710, Portugal.

Color versions of one or more of the figures in this paper are available online at http://ieeexplore.ieee.org.

Digital Object Identifier 10.1109/JSEN.2009.2026520

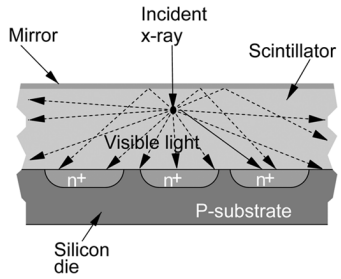

Fig. 1. X-ray detector representation with a scintillator layer placed on top of a photodetector array.

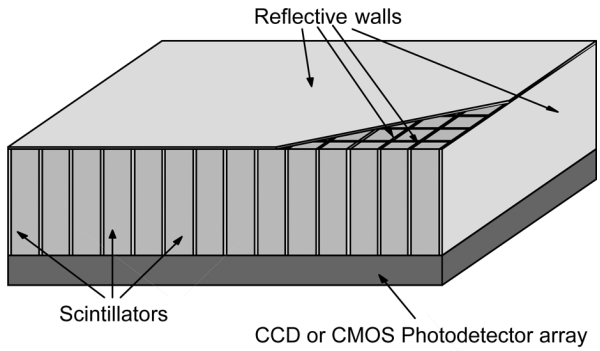

Fig. 2. Schematic representation of the detector structure.

Instead of a single scintillation layer on top of the photodetector array, a microcolumnar structure scintillator screen can be used. The microcolumnar structure is produced by the vapor deposition of the scintillator on a fiberoptic faceplate. This structure reduces the lateral spreading of optical light [3]. With this approach, the scintillator thickness can be increased.

As an alternative approach, by placing the scintillators separated by reflective surfaces, the thickness of the scintillator can be increased without decreasing the spatial resolution (Fig. 2) [4]. With this sensor geometry, the light yield by each scintillator is guided to the corresponding photodetector by the reflective walls. The constraints associated with this coupling method have been studied by the authors in the previous work [5]. Also, the aluminum has been studied as the reflection layer material and the CsI:Tl as the scintillator material.

Fig. 3 shows a cross section of a scintillator-based X-ray detector with three channels or pixels. The CsI:Tl scintillator must be coated by a reflective layer (reflector in Fig. 3), allowing that

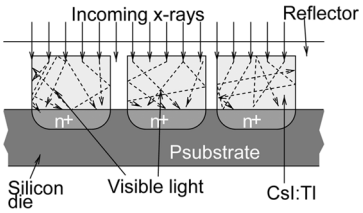

Fig. 3. Cross section of a scintillator-based X-ray detector with three channels or pixels.

the X-rays go trough the crystal and not allowing that the generated visible light escapes to the outside, driving therefore the light to the photodetector ($\mathrm{n}+/\mathrm{p}$-substrate junction in Fig. 3).

The most critical steps that can affect the efficiency and the signal-to-noise ratio (SNR) of such a detector are the following:

- transmission of the X-rays through the reflective layer;
- absorption of the X-rays by the scintillator and their conversion into visible light;
- reflection of the visible light by the reflective layer;
- transmission of the visible light to the photodetector;
- detection of the visible light by the photodetector and further conversion into an electrical signal.

The following considerations should be pointed out.

1) The most common noise sources in pixel detectors for X-ray imaging systems are the photonic noise, fixed pattern noise, and readout electronics noise [6]. The fixed pattern noise is a characteristic of all pixel array sensors and can be canceled by the use of gain maps [7]. The noise of the readout electronics depends mainly on the circuit configuration and layout and usually is less important than the photonic noise.
2) The photonic noise, which is caused by the statistical distribution of the X-ray photons in time and space, is the fundamental noise limit of an X-ray detector. Several theoretical analysis and experiments have shown that the intrinsic photonic noise of an X-ray beam is random and follows a Poisson distribution; that is, the standard deviation σ_{prx} is equal to the square root of the average number of X-ray photons m_{prx} [8], [9], such that

$$\sigma_{\mathrm{prx}} = \sqrt{m_{\mathrm{prx}}} \tag{1}$$

and the SNR is given by

$$\mathrm{SNR} = \frac{m_{\mathrm{prx}}}{\sigma_{\mathrm{prx}}} = \sqrt{m_{\mathrm{prx}}}. \tag{2}$$

3) A scintillator converts the absorbed energy into visible light. In the case of the CsI:Tl used in this work, it produces about 65 900 visible photons for each 1 MeV of absorbed energy, at room temperature [10]; that is, for each photon of 1 MeV, it produces a random number of photons whose average is 65 900. Therefore, the average amount of produced light for a given X-ray energy, $L_R(E)$, is obtained by the product of five factors, namely: a) the number of incident X-ray photons m_{prx}, which is a random quantity; b) the transmissivity of the reflective layer on top of the scintillator, $\mathrm{Tr}_{\mathrm{ref}}$ (Figs. 1–3); c) the absorption of the scintillator, $\mathrm{Ab}_{\mathrm{sc}}$; d) 65 900 photons/MeV, which is the mean value of a random process; and e) the energy of each X-ray photon, E. Thus

$$L_R(E) = m_{\mathrm{prx}} \times \mathrm{Tr}_{\mathrm{ref}} \times \mathrm{Ab}_{\mathrm{sc}} \times 65\,900 \times E. \tag{3}$$

In this case, the variance of the produced photon distribution, $\sigma^2_{LR}(E)$, is given by the product of the mean value of the photons absorbed by the scintillator by the square of the number of visible photons produced in the scintillator for each incident X-ray photon, such that

$$\sigma^2_{LR}(E) = m_{\mathrm{prx}} \times \mathrm{Tr}_{\mathrm{ref}} \times \mathrm{Ab}_{\mathrm{sc}} \times (65\,900 \times E)^2. \tag{4}$$

This result is in accordance with previously presented works [11], [12].

The SNR can be calculated for each energy and is given by

$$\mathrm{SNR}(E) = \frac{L_R(E)}{\sigma_{LR}(E)} = \sqrt{m_{\mathrm{prx}} \times \mathrm{Tr}_{\mathrm{ref}} \times \mathrm{Ab}_{\mathrm{sc}}}. \tag{5}$$

When comparing (2) with (5), one can conclude that, despite the photon multiplication that occurs in the scintillator, the SNR decreases once $\mathrm{Tr}_{\mathrm{ref}}$ and $\mathrm{Ab}_{\mathrm{sc}}$ are both lower than 1. However, $\mathrm{Ab}_{\mathrm{sc}}$ can be increased by increasing the thickness of the scintillator, but this solution also increases the cross talk between neighbor pixels. By using a structure similar to the one shown in Figs. 2 and 3, it is possible to increase the scintillator thickness without increasing the cross talk.

A few methods to fabricate structures similar to the one shown in Figs. 2 and 3 have been described [4], [13]–[17]. The fabrication processes described in previous works, featuring architectures based on light guides, are based on diverse techniques such as the fabrication of microcavities, which are then filled with scintillating material. The cavities can be fabricated by chemical etching [15], laser ablation [16], or by deep reactive ion etching [17]. The opposite is also possible: opening cavities in a scintillating crystal and filling them with reflective material [18]. The present work distinguishes from these solutions in the fabrication technique of the scintillating matrix embedded in reflective walls. In this case, it is based on a photolithographic process, where a SU-8 sacrificial layer is used, allowing its quick fabrication and placement on top of the photodetector matrix.

II. Device Design

The fabrication steps of this X-ray detector design featuring scintillators inside light guides and an array of photodetectors underneath consist briefly in: producing a detailed square islands pattern on SU-8 over the photodetector array; deposition of aluminum which will fill the spaces within the pattern; complete removal of the SU-8; scintillator placement inside the cavities formed by the removal of SU-8; and an aluminum layer deposition on the top of the structure.

In this work, the photodetectors consist of a commercially available array of CMOS photodiodes ($\mathrm{n}+/\mathrm{p}$-substrate junctions). The chosen scintillator was thallium-doped cesium iodide (CsI:Tl), due to its high light yield, relatively high density and atomic number of its elements, which is necessary in order to absorb the X-rays [19]. The thallium concentration should be around 0.03 m/o and the evaporation rate 4 μm/min [20].

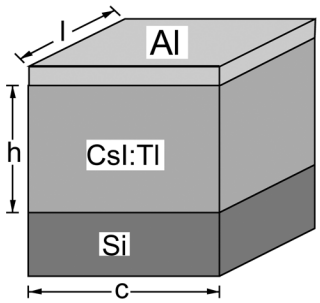

Fig. 4. Scintillator on the top of a silicon photodetector.

As previously mentioned, a reflective material is used to coat the scintillator. It works like a light guide avoiding visible light dispersion and interference between each neighbor pixel, thus minimizing cross-talking [19]. Moreover, it improves the spatial resolution, as well as it increases the intensity of the transmitted light to the photodetectors. Due to these issues, the amount of the incoming X-ray radiation can be reduced while keeping the same sensitivity of the photodetectors signal readout.

So, with this geometry, the X-rays cross first the reflective material placed on the top and reach the scintillator, where they are absorbed. For each X-ray absorbed photon, many visible light photons are produced, traveling in all directions. Some of them arrive directly at the photodetector, while others reach the reflector. After some reflections, disregarding the losses in the mirror, almost all the visible light photons reach the photodetector.

It was chosen aluminum for the reflective walls since this material has relatively low density and low atomic number, thus allowing the penetration of the X-rays [19].

A. Comparison of the Efficiency of the Scintillator With and Without Light Guides

Consider Fig. 4 that represents only 1 pixel of the image detector of Fig. 1. The top surface of the scintillator is coated by a reflective material that forms the mirror for the visible light produced by the scintillator and prevents visible light to enter from the outside producing undesirable noise in the detector. When an X-ray photon is absorbed by the scintillator, it produces an amount of visible light (L_R).

The relationship between the area of scintillator seen by the photodetector, a, and the total area of its surface, A, is defined by

$$R_a = \frac{a}{A} \tag{6}$$

where $a = lc$ and $A = 2lc + 2hc + 2lh$. Considering that the scintillator is transparent and emits light uniformly in all directions, the amount of light that reaches directly the photodetector without reflections is given by

$$L_1^* = L_R R_a (1 - R_{\rm pd}) \tag{7}$$

where $R_{\rm pd}$ is the reflectivity of the photodetector surface.

It is considered that all the points of the mirror on the top of the scintillator are at the same distance of the photodetector, i.e., the mirror, instead of being plane, is the area of a spherical surface, whose radius is given by h. In this case, the light reflected at the photodiode surface that reaches the mirror is given by

$$L_{M1}^* = L_R R_a R_{\rm pd} \frac{a}{2\pi h^2}. \tag{8}$$

The percentage of light that is lost in the mirror is $R_{\rm loss}$. In this case, the light that leaves the mirror and comes back to the photodiode is given by

$$L_2^* = L_{M1}^* (1 - R_{\rm loss}) \frac{a}{2\pi h^2} (1 - R_{\rm pd}). \tag{9}$$

Once again, a percentage of the light is reflected at the photodiode surface and goes back again to the mirror, which reflects it again, and so on. The total amount of light that is absorbed by the photodetector is given by the sum

$$\begin{aligned} L^* &= L_1^* + L_2^* + \cdots + L_n^* \\ &= \sum_{i=0}^{\infty} L_R R_a (1 - R_{\rm pd}) R_{\rm pd}^i (1 - R_{\rm loss})^i \left(\frac{a}{2\pi h^2}\right)^{2i}. \end{aligned} \tag{10}$$

On the other hand, the light produced by the scintillator can go directly to the mirror, where it is reflected back to the photodiode and so on. The light that is absorbed by the photodiode in this way is given by

$$\begin{aligned} L^{**} &= L_1^{**} + L_2^{**} + \cdots + L_n^{**} \\ &= \sum_{i=0}^{\infty} L_R R_a (1 - R_{\rm pd}) R_{\rm pd}^i (1 - R_{\rm loss})^{i+1} \left(\frac{a}{2\pi h^2}\right)^{2i+1}. \end{aligned} \tag{11}$$

The total amount of light, $L = L^* + L^{**}$, is obtained by adding (10) with (11), and after mathematical handling, it can be written as a function of L_R as

$$\frac{L}{L_R} = \frac{2\pi h^2 R_a (a + 2\pi h^2 - a R_{\rm loss})(1 - R_{\rm pd})}{4\pi^2 h^4 + a^2 (1 - R_{\rm loss}) R_{\rm pd}}. \tag{12}$$

A similar deduction was made for the model of Fig. 3 and presented in [5]. The result is given by

$$\frac{L}{L_R} = \frac{R_a (1 - R_{\rm pd})}{1 - (1 - R_a (1 - R_{\rm pd}))(1 - R_{\rm loss})}. \tag{13}$$

As a practical example, consider that the reflectivity of the photodiode surface is 5%, the losses at the mirror are 15%, $h = 100$, $c = 30$, and $l = 30$ μm. In this case, (12) gives a percentage of absorbed light of 6.27%, while (13) gives a percentage of absorbed light of 30.57%. This means that by introducing the light guides, the efficiency of the detector is substantially increased.

III. Device Fabrication

Sacrificial layers of MicroChem OmniCoatTM and SU-8 photoresist are spun over the CMOS photodetector array [Fig. 5(a)]. SU-8 was chosen as it enables deep structures with very low sidewall roughness, which is suitable for the required cavities. Moreover, the patterning of the SU-8 implies a low-cost process.

- The MicroChem SU-8 100 was used. Using a final rotation speed of 2900 rpm, a thickness of about 120 μm was obtained.

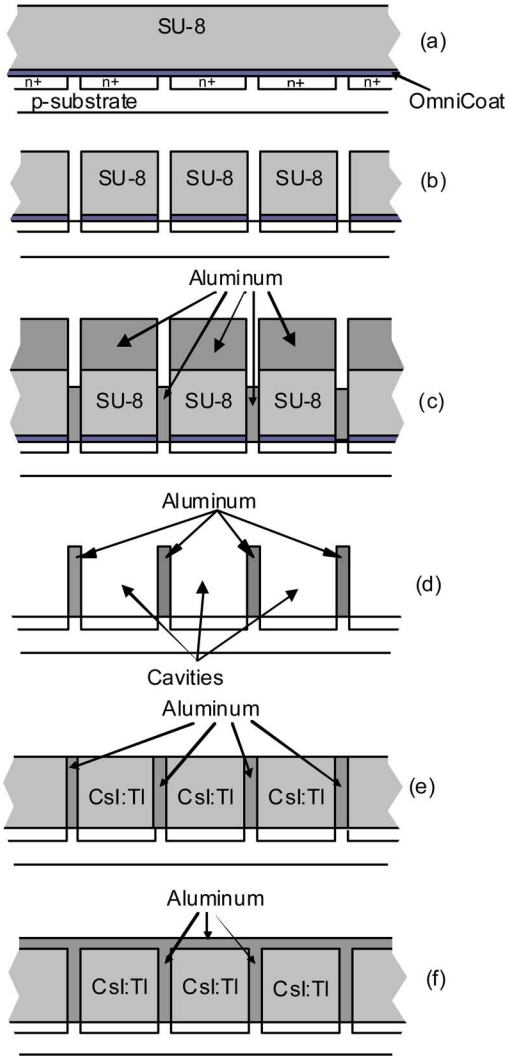

Fig. 5. Fabrication steps of the scintillating light guides [19]: (a) the CMOS photodetectors array is spin coated with OmniCoat and SU-8; (b) after exposure to UV light through an appropriate mask, suitable solvents are used to dissolve the unexposed resist and the OmniCoat; (c) an aluminum layer is deposited over the entire array; (d) SU-8 and OmniCoat are removed along with the aluminum on top of it; (e) the scintillator is placed inside the cavities and polished; and (f) a final aluminum layer is deposited.

- The soft bake program followed was 10 min at 65 °C, 120 min at 95 °C, and cooling down above the hot plate for 1 h. The samples were allowed to relax residual stresses over night.
- In the exposure setup that was used, the optimum exposure time was 60 s. A quartz mask was used in this step.
- Postexposure bake was performed at 95 °C for 20 min, followed by cooling down on the hot plate for 1 h.
- The samples were developed for 10 min on MicroChem Developer.

The SU-8 is exposed to UV light through an appropriate mask with the desired cavity geometry and dimensions, and after exposure, a suitable solvent (MicroChem Developer) dissolves the unexposed resist. SU-8 columns are formed on top of the photodetectors. After this step, the OmniCoat was also developed with Microposit MF-319 Developer [Fig. 5(b)].

The next step is to deposit, by physical vapor deposition (PVD), the aluminum layer over the entire array [Fig. 5(c)].

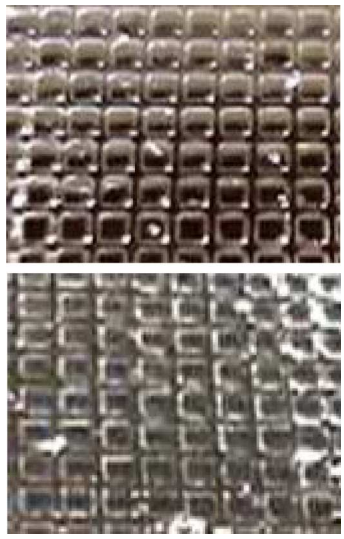

Fig. 6. Images obtained after aluminum deposition (on top) and after removal of SU-8 (below).

A 100-μm-thick aluminum layer was deposited. After that, the SU-8 and the OmniCoat are removed with the MicroChem Remover PG, as well as the aluminum on top of those columns [Fig. 5(d)].

Following, the scintillators are placed inside the cavities by PVD [Fig. 5(e)]. The dimensions of each scintillator are 30 μm $\times$ 30 μm $\times$ 100 μm and the aluminum walls are 6 μm thick, so the pixel size is 36 μm $\times$ 36 μm.

Finally, an aluminum layer is deposited again, by PVD, on top of the scintillator [Fig. 5(f)]. This step is performed after a polishing procedure in order to remove the CsI:Tl deposited on top of the aluminum walls, as well as to get an uniform surface with low surface roughness, eliminating irregularities.

The CMOS detector array has 120×106 pixels with 36 μm $\times$ 36 μm pixel size.

IV. Experimental Setup and Results

A. Experimental Equipments

- Spin coater (Laurell Technologies WS-650 LITE Series Spin Processor).
- Precision hot plate (Präzitherm PZ 28-2 EB, from Harry Gestigkeit GmbH).
- UV exposure equipment (Karl Suss MJB3 Mask Aligner).
- PVD equipment (Edwards 306).
- Optical microscope (NIKON) with color video camera (SONY CCD-IRIS) and computerized workstation with DVTools.
- X-ray equipment (PHILIPS X'Pert).

B. Results

Fig. 6 shows two images obtained after aluminum deposition (on top) and after removal of SU-8 (below).

Fig. 7 shows a picture of the prototype.

The main difficulty encountered was the complete removal of unexposed SU-8 from the narrow cavities where the aluminum was to be deposited in. The optimum developing of SU-8 revealed itself somewhat difficult. The consequences are, in the

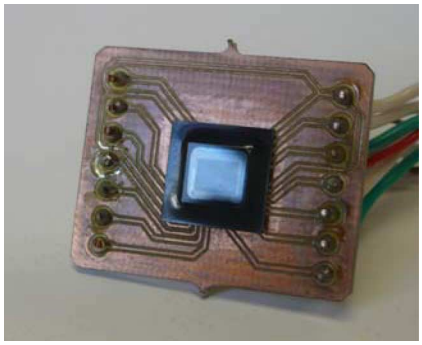

Fig. 7. X-ray image detector prototype.

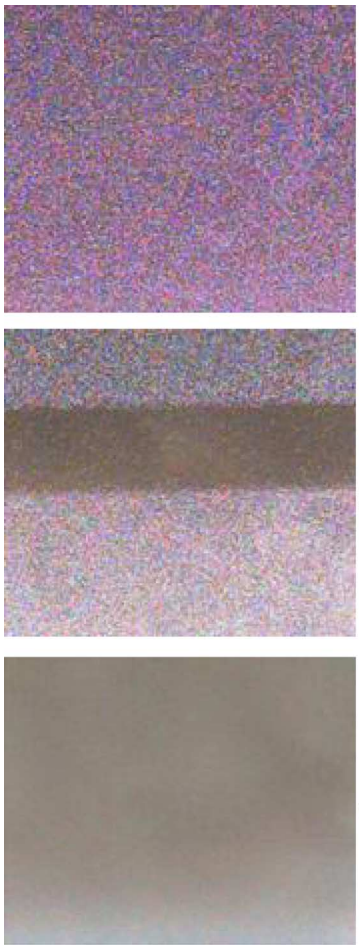

Fig. 8. Images obtained (a) without and (b) with a pin in the X-ray beam path, and also with the X-ray source (c) turned of.

lift-off step, the release of aluminum, which might have been deposited in SU-8 residue. This fact was improved by using the OmniCoat in an ultrasonic bath.

X-ray tests were performed using the PHILIPS X'Pert equipment. The sensor with the CsI:Tl and the aluminum layers was placed in the path of the X-ray beam and connected to a computer via USB port. This procedure was repeated with a pin of 0.5 mm diameter placed close to the chip in the X-ray path (Fig. 8). For all the tests, the X-ray tube equipment was powered with 50 kV and 1 mA, the sensor was placed 20 cm down from the tube, the exposure time was 1/30 s, and the A/D converter of the sensor has a resolution of 10 bits.

In Fig. 8, it is possible to observe a small amount of noise. This noise can be ascribed to two main effects: some X-rays crossing the scintillator or the aluminum walls and hitting directly on the CMOS detectors and/or differences in pixel fabrication (fixed pattern noise). These issues can be solved by increasing the thickness of the scintillator, by avoiding placing the photodetector active area below the aluminum walls and by using fixed pattern noise compensation.

The SNRs were calculated for Fig. 8(a) and (c), and the obtained values are as follows:

Fig. 8(a) –> $\mathrm{SNR} = 17.58$ dB.

Fig. 8(c) –> $\mathrm{SNR} = 21.58$ dB.

The SNR was calculated using an equation similar to (2), where the mean value of the brightness of all the pixels was placed in the numerator and the standard deviation in the denominator. The values of SNR can be increased with image processing techniques (not used here) such as contrast and brightness balance.

V. Conclusion

The spatial resolution of X-ray detectors based on scintillating crystals for digital radiography can be improved by confining the scintillator with a reflective material such as aluminum. It was explained as a method for preparing cavities of reflective material, where the scintillator will be placed, which has the advantages of being a low-cost method that performs regular shape, resulting in homogeneity and reproducibility of the cavities. Once the cavities are fabricated, the scintillator can be simply evaporated into the cavities.

The prototype obtained supports the method described and the preliminary results are promising.

References

[1] J. Yorkston, "Recent developments in digital radiography detectors," *Nucl. Instrum. Methods Phys. Res.*, vol. A 580, pp. 974–985, 2007.

[2] J. G. Rocha and S. Lanceros-Mendez, "X-ray imaging matrix with light guides and intelligent pixel sensors, radiation or high energy particle detector devices that contain it, its fabrication process and its use," Patent WO2007046010, 2007.

[3] V. V. Nagarkar, S. V. Tipnis, T. K. Gupta, S. R. Miller, V. B. Gaysinskiy, Y. Klugerman, M. R. Squillante, G. Entine, and W. W. Moses, "High speed X-ray imaging camera using a structured CsI(Tl) scintillator," *IEEE Trans. Nucl. Sci.*, vol. 46, no. 3, pp. 232–236, Jun. 1999.

[4] P. Kleimann, J. Linnros, C. Frojdh, and C. S. Petersson, "An x-ray imaging pixel detector based on a scintillating guides screen," *IEEE Trans. Nucl. Sci.*, vol. 47, pp. 1483–1486, Aug. 2000.

[5] J. G. Rocha and S. Lanceros-Mendez, "3-D modeling of scintillator-based X-ray detectors," *IEEE Sensors J.*, vol. 6, no. 5, pp. 1236–1242, Oct. 2006.

[6] E. Dubaric, C. Fröjdh, H. E. Nilsson, and C. S. Petersson, "Resolution noise and properties of scintillator coated X-ray detectors," *Nucl. Instrum. Methods Phys. Res. A, Accel. Spectrom. Detect. Assoc. Equip.*, vol. 466, no. 1, pp. 178–182, 2001.

[7] R. Irsigler, J. Andersson, J. Alverbro, J. Borglind, C. Fröjdh, P. Helander, S. Manolopoulus, H. Martijn, V. O'Shea, and K. Smith, "X-ray imaging using a 320 × 240 hybrid GaAs pixel detector," *IEEE Trans. Nucl. Sci.*, vol. 46, no. 3, pp. 507–512, Jun. 1999.

[8] A. Workman and D. S. Brettle, "Physical performance measures of radiographic imaging systems," *Dentomaxillofacial Radiol.*, vol. 26, no. 3, pp. 139–146, 1997.

[9] M. W. Tate, E. F. Eikenberry, S. L. Barna, M. E. Wall, J. L. Lowrance, and S. M. Gruner, "A large-format high-resolution area X-ray detector based on a fiber-optically bonded charge-coupled device (CCD)," *J. Appl. Crystallogr.*, vol. 28, pp. 196–205, 1995.

[10] J. Valentine, D. Wehe, G. Knoll, and C. Moss, "Temperature dependence of absolute CsI(Tl) scintillation yield," in *Proc. IEEE Nucl. Sci. Symp. Conf. Rec.*, 1991, pp. 176–182.
[11] S. M. Gruner, M. W. Tate, and E. F. Eikenberry, "Charge coupled device area X-ray detectors," *Rev. Sci. Instrum.*, vol. 73, no. 8, pp. 2815–2842, 2002.
[12] R. K. Swank, "Absorption and noise in X-ray phosphors," *J. Appl. Phys.*, vol. 44, no. 9, pp. 4199–4203, 1973.
[13] C. P. Allier, R. W. Hollander, C. W. E. van Eijk, P. M. Sarro, M. de Boer, J. B. Czirr, J. P. Chaminade, and C. Fouassuier, "Thin photodiodes for a neutron scintillator silicon-well detector," *IEEE Trans. Nucl. Sci.*, vol. 48, pp. 1154–1157, Aug. 2001.
[14] J. G. Rocha, C. G. J. Schabmueller, N. F. Ramos, S. Lanceros-Mendez, M. F. Costa, A. G. R. Evans, R. F. Wolffenbuttel, and J. H. Correia, "X-ray detector based on a bulk micromachined photodiode combined with a scintillating crystal," *J. Micromech. Microeng.*, vol. 13, pp. S45–S50, 2003.
[15] S. Xiao-Dong, "X-ray detectors with a grid structured scintillators," Patent US2004251420, 2004.
[16] V. V. Nagarkar and S. V. Tipnis, "Pixellated micro-columnar film scintillator," Patent US2004042585, 2004.
[17] P. Sture, L. Jan, and F. Christer, "X-ray pixel detector device and fabrication method," Patent US 6 744 052, 2004.
[18] D. H. T. Von, "X-ray detector array and method for manufacturing same," Patent US2002163992, 2002.
[19] J. G. Rocha, G. Minas, L. M. Goncalves, and S. Lanceros-Mendez, "Scintillating microcavities for x-ray imaging sensors," in *Micro Mech. Eur. Workshop*, Sept. 2006, pp. 149–152.
[20] I. Fujieda, G. Cho, J. Drewery, T. Gee, T. Jing, S. N. Kaplan, V. Perez-Mendez, D. Wildermuth, and R. A. Street, "X-ray and charged particle detection with CsI(Tl) layer coupled to a a-Si:H photodiode layers," *IEEE Trans. Nucl. Sci.*, vol. 38, pp. 255–262, Apr. 1991.

J. G. Rocha received the B.Sc., M.Sc., and Ph.D. degrees in industrial electronics engineering from the University of Minho, Guimarães, Portugal, in 1995, 1999, and 2004, respectively.

He was a Visiting Researcher at the Delft University of Technology, The Netherlands, in 2001–2002. Since 2004, he has been an Assistant Professor with the Department of Industrial Electronics, University of Minho, where he is involved in research on sensors and sensor interfaces.

R. A. Dias received the M.Sc. degree in biomedical engineering from the University of Minho, Braga, Portugal, in 2007.

She has attended a medical electronics directed education and performed research on optical microsensors for biomedical applications.

L. Gonçalves received the Graduate degree in 1993, and the M.Sc. and Ph.D. degrees, both in electronics engineering, from the University of Minho, Guimarães, Portugal, in 1999 and 2008, respectively.

From 1993 to 2002, he researched on embedded systems and electronics, on Idite-Minho, an Institute to interface between university and industry, Braga, Portugal. Since 2002, he teaches at Electronics Department, University of Minho, where he is an Assistant Professor since 2008. There, he started a new lab on thermoelectric thin-film deposition, characterization, and patterning, in collaboration with Physics department. Currently, he is involved in the research on thermoelectric materials for on-chip cooling and energy harvesting. His research interests include thermoelectrics, microfabrication technology, and microsystems.

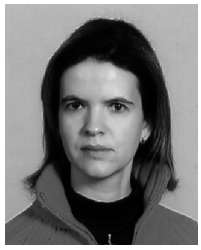

G. Minas (S'96–M'09) received the B.Sc. degree in industrial electronics engineering and the M.Sc. and Ph.D. degrees from the University of Minho, Guimarães, Portugal, in 1994, 1998, and 2004, respectively.

Her thesis work was in cooperation with the Laboratory for Electronic Instrumentation, Delft University of Technology, Delft, The Netherlands, and dealt with lab-on-a-chips for biological fluids analysis. From 1995 to 2004, she was a Lecturer with the Department of Industrial Electronics, University of Minho, where she has been an Assistant Professor since 2004. At the university, she is involved in biomedical microdevices research.

Dr. Minas won second place for the Best Oral Presentation at Eurosensors XVII.

A. Ferreira received the Graduate degree in physics from the University of Minho, Braga, Portugal, in 2007. He is currently working towards the M.Sc. degree at the University of Minho.

Since October 2007, he has been a Researcher at the Physics Department, University of Minho, Portugal. His research interests include electroactive smart materials and multifunctional films for flexible and plastic material applications.

C. M. Costa received the Graduate degree in physics, and the Masters degree in materials engineering, from University of Minho, Braga in 2005 and 2007, respectively.

Currently, he is a member of the research group in Electroactive Materials and Cooperative Phenomena in Dielectrics, University of Minho, Braga, Portugal, and a member of the Smart Materials Group at CeNTI, leading activities in a wide range of materials processing (mainly chemical processing) and respective characterization, specially at micro- and nanoscale structural and characterization of materials using scanning probe and atomic force microscopy and also magnetic force microscopy, piezoresponse force microscopy, and electric force microscopy.

S. Lanceros-Mendez received the B.Sc. degree in physics from the University of the Basque Country, Leioa, Spain, in 1991, and the Ph.D. degree from the Institute of Physics, Julius-Maximilians-Universität, Würzburg, Germany, in 1996.

He was a Research Scholar with Montana State University, Bozeman, from 1996 to 1998. Since September 1998, he has been with the the Department of Physics, University of Minho as an Associate Professor, where he is involved in experimental investigations in the area of condense matter physics and its applications. He was a Visiting Researcher at the A. F. Ioffe Physico-Technical Institute, Russia, in 1995, the University of Porto, Portugal, in 1996, Pennsylvania State University, Philadelphia, in 2007, and the University of Potsdam, Germany, 2008.